Photosynth Res
DOI 10.1007/s11120-017-0453-0

ORIGINAL ARTICLE

Engineering a carotenoid-binding site in *Dokdonia* sp. PRO95 Na^+-translocating rhodopsin by a single amino acid substitution

Viktor A. Anashkin[1] · Yulia V. Bertsova[1] · Adalyat M. Mamedov[1] · Mahir D. Mamedov[1] · Alexander M. Arutyunyan[1] · Alexander A. Baykov[1] · Alexander V. Bogachev[1]

Received: 14 August 2017 / Accepted: 29 September 2017

Abstract Light-driven H^+, Cl^- and Na^+ rhodopsin pumps all use a covalently bound retinal molecule to capture light energy. Some H^+-pumping rhodopsins (xanthorhodopsins; XRs) additionally contain a carotenoid antenna for light absorption. Comparison of the available primary and tertiary structures of rhodopsins pinpointed a single Thr residue (Thr216) that presumably prevents carotenoid binding to Na^+-pumping rhodopsins (NaRs). We replaced this residue in *Dokdonia* sp. PRO95 NaR with Gly, which is found in the corresponding position in XRs, and produced a variant rhodopsin in a ketocarotenoid-synthesising *Escherichia coli* strain. Unlike wild-type NaR, the isolated variant protein contained the tightly bound carotenoids canthaxanthin and echinenone. These carotenoids were visible in the absorption, circular dichroism and fluorescence excitation spectra of the Thr216Gly-substituted NaR, which indicates their function as a light-harvesting antenna. The amino acid substitution and the bound carotenoids did not affect the NaR photocycle. Our findings suggest that the antenna function was recently lost during NaR evolution but can be easily restored by site-directed mutagenesis.

Keywords Rhodopsin · Na^+ pump · Carotenoid antenna · Canthaxanthin · Echinenone · Xanthorhodopsin

Abbreviations

CAN	Canthaxanthin
CD	Circular dichroism
DDM	*n*-Dodecyl β-D-maltoside
ECN	Echinenone
Kr2	Na^+-translocating rhodopsin of *Krokinobacter eikastus*
MD	Molecular dynamics
NaR	Na^+-translocating rhodopsin of *Dokdonia* sp. PRO95
RMSD	Root mean square deviation
SX	Salinixanthin
T216G-NaR	Thr216Gly variant of NaR
XR	Xanthorhodopsin

Introduction

Two essentially different transducers can convert solar energy, the key factor of the biosphere: chlorophyll-containing reaction centres (photosystems) and retinal-containing proteins, such as bacteriorhodopsin, halorhodopsin and Na^+-translocating rhodopsin. Chlorophyll-containing photosystems compensate for the low intensity of sunlight at the surface of the Earth by the presence of light-harvesting antennae. These antennae widen the spectral and polarisation range of the absorbed light and markedly increase the cross-section for light absorption by the photosynthetic reaction centres (Croce and Amerongen 2014). In contrast, most retinal-containing proteins lack light-harvesting components.

However, the simplest light-harvesting antenna formed by a single carotenoid molecule has recently been discovered in the bacteriorhodopsin homologue xanthorhodopsin (XR), which is found in the bacterium *Salinibacter ruber* (Balashov et al. 2005). The XR carotenoid transfers the energy of the absorbed photon to retinal, which further converts the energy into a proton potential difference (Balashov et al.

✉ Alexander V. Bogachev
bogachev@belozersky.msu.ru

[1] Belozersky Institute of Physico-Chemical Biology, Lomonosov Moscow State University, Moscow, Russia 119234

Published online: 05 October 2017

2005; Boichenko et al. 2006). The XR antenna is formed by salinixanthin (SX; Fig. 1), which is the major carotenoid of *S. ruber*, bound at a 1:1 stoichiometric ratio (Balashov et al. 2005). The site of carotenoid binding and its amino acid ligands have been identified by X-ray diffraction analysis of XR (Luecke et al. 2008), which revealed that the terminal ring groups of the carotenoid and retinal are in close proximity to each other. The carotenoid antenna can be removed from XR and reconstituted *in vitro* upon incubation of the depleted protein with the carotenoids (Balashov et al. 2006; Imasheva et al. 2011). In addition to XR of *S. ruber*, heterologously produced carotenoid-free proton-pumping rhodopsin of the cyanobacterium *Gloeobacter violaceus* can bind the *G. violaceus* carotenoid echinenone (ECN; Fig. 1), which functions as a light-harvesting antenna (Balashov et al. 2010).

However, Cl^-- and Na^+-transporting rhodopsins (Inoue et al. 2013) are less characterised in this respect. The three-dimensional structure of the Na^+-rhodopsin from the marine flavobacterium *Krokinobacter eikastus* (Kr2) (Gushchin et al. 2015; Kato et al. 2015) is very similar to that of XR, including its carotenoid-binding site. This site was unoccupied in the crystal structure of Kr2 produced in *E. coli* cells that are unable to synthesise carotenoids. Nevertheless, Kr2 was assumed to contain a carotenoid antenna in the cells of its host, *K. eikastus* (Gushchin et al. 2015; Kato et al. 2015). However, attempts to reconstitute a similar light-harvesting antenna in the Na^+-rhodopsin (NaR) of another marine flavobacterium, *Dokdonia* sp. PRO95, have been unsuccessful (Bertsova et al. 2016). Both SX and the total carotenoid pool of *Dokdonia* were used in these reconstitution trials. Interestingly, *Dokdonia* sp. PRO95 NaR is very similar to Kr2 (98% residue identity) and contains all the residues of the Kr2 putative carotenoid-binding site (Bertsova et al. 2016).

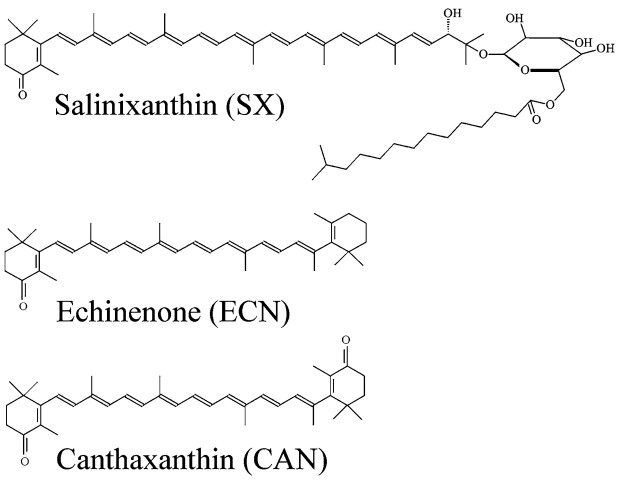

Fig. 1 Chemical structures of three ketocarotenoids

Taken together, these data suggest that carotenoid antennae are absent in flavobacterial Na^+-rhodopsins. The experiments described below aimed to understand the structural basis for this phenomenon and its evolutionary conditionality.

Materials and methods

Site-directed mutagenesis and expression of the *Dokdonia* sp. PRO95 NaR gene (GenBank code: AEX55013)

To produce the Thr216Gly mutation in NaR (T216G), the following direct mutagenic primer was used: 5′-TTTTTA ATATCGTGGggTTTATATCCAGGCGCTTACTTAA (the lowercase letters indicate the substituted nucleotides); the reverse primer was complementary to the direct primer. Mutagenesis was performed using a QuikChange II kit (Stratagene) and the plasmid pRhod_10.1 (Bertsova et al. 2015) as a template, resulting in a pRhod_T216G plasmid. The NaR-encoding region of pRhod_T216G was verified using DNA sequencing.

The pRhod_T216G plasmid and the intact pRhod_10.1 plasmid harbouring the wild-type NaR gene were transformed into *E. coli* BL21 or *E. coli*/pACCAR25ΔcrtXZcrtO cells (Moldenhauer et al. 2017). The cells were grown at 37 °C in a terrific broth medium to the late exponential phase ($A_{600} \approx 1.5$), after which the growth medium was supplemented with 0.15% (w/v) L-arabinose and 1.5 mg/L all-*trans* retinal. The cells were further grown for 16 h at 15 °C and then harvested by centrifugation (10,000 *g*, 10 min).

Purification of wild-type and variant NaRs

Recombinant 6 × His-tagged NaR and its T216G variant were isolated using metal-chelating chromatography as described previously (Bertsova et al. 2015). The proteins were quantified by their absorbance at 523 nm upon bleaching in the presence of hydroxylamine (Mamedov et al. 2016).

Extraction of carotenoids

The carotenoids of *S. ruber* and *E. coli*/pACCAR25ΔcrtXZcrtO/pRhod_T216G were extracted from the corresponding bacterial cells; an acetone:methanol (7:3, v/v) mixture was used for the extractions, after which the carotenoids were transferred to hexane by the addition of water/hexane. The hexane solution was evaporated, and the residue was redissolved in acetone. Phospholipids were removed from the extract by several cycles of precipitation with cold acetone (Hsieh et al. 1974).

The procedure to extract carotenoids from the T216G-NaR was essentially identical. Prior to the extraction, the protein was precipitated using ammonium sulphate, and the floating precipitate was washed with a saturated ammonium sulphate solution.

Spectral measurements

Optical absorption spectra were measured using an Agilent 8453 spectrophotometer. The following values of extinction coefficients (mM^{-1} cm^{-1}) were used for quantification: SX in methanol, 140 at 480 nm (Imasheva et al. 2008); ECN in petroleum ether, 119 at 488 nm (Britton et al. 2004); and canthaxanthin (CAN) in petroleum ether, 124 at 466 nm (Britton et al. 2004). Circular dichroism (CD) spectra were recorded using a Chirascan CD spectrometer (Applied Photophysics).

Fluorescence emission and excitation spectra were recorded using a FluoroMax-3 spectrofluorometer (Horiba Jobin Yvon). The protein concentration was 1 µM, and the sample absorbance at all wavelengths used did not exceed 0.1. Emission spectra were recorded according to the excitation at 565 nm; the bandwidths of the emission and excitation channels were 5 and 10 nm, respectively. Excitation spectra were recorded using an emission wavelength of 670 nm and emission and excitation bandwidths of 10 and 4 nm, respectively. Excitation spectra were corrected for the wavelength dependence of the intensity of the excitation light and for Raman scattering from the buffer.

Flash photolysis measurements of the NaR photocycle

Light-induced absorbance changes of NaR were recorded as described previously (Mamedov et al. 2016). The time courses of absorbance were fitted as three consecutive irreversible steps (Mamedov et al. 2016). The sodium contamination of the assay media used in the flash photolysis experiments was measured using flame photometry.

Thin-layer chromatography

Carotenoids were separated on silica gel plates (Sorbfil, 15 × 15 cm); an acetone:hexane (1:4, v/v) solution was used as the mobile phase. The bands were eluted, and the carotenoids present in them were identified based on their absorption spectra (Britton et al. 2004). The R_f values for CAN and ECN were 0.69 and 0.91, respectively, in our system.

Molecular dynamics (MD)

MD simulations were performed with one subunit of XR. The other subunit and all small organic molecules were removed from the structure of the XR homodimer (PDB ID: 3DDL) (Luecke et al. 2008). A virtual Gly201Thr mutation was performed using the program UCSF Chimera (Pettersen et al. 2004). XR structures were placed into a symmetrical bilayer membrane using CHARMM-GUI (Jo et al. 2008; http://www.charmm-gui.org); each layer was formed by 25 molecules of 1-palmitoyl-2-oleoyl-*sn*-glycero-3-phosphocholine and 75 molecules of 1-palmitoyl-2-oleoyl-*sn*-glycero-3-phosphoethanolamine. The membrane was solvated with 29 Å of water molecules at each membrane side in a final box volume of approximately 770,000 $Å^3$. Finally, the systems were supplemented with 42 Cl^- and Na^+ ions each, corresponding to a 0.15 M NaCl solution, using CHARMM-GUI.

MD simulations were performed using the PMEMD program (CUDA implementation) of the AMBER 14 software suite and the ff14SB and lipid14 force fields (Case et al. 2014; http://ambermd.org). The general AMBER force field of the same suite was used for the retinal residue and SX. The total number of atoms in the simulations was approximately 71,000. The systems were minimised and equilibrated using the standard initial parameters generated at the final CHARMM-GUI modelling step with simultaneous heating to 303 K and the cancellation of boundary restraints. Temperature was maintained using a Langevin thermostat. A 10-Å cut-off MD production was performed for 200 ns, and snapshots were saved every 2 ps. Postprocessing trajectory analyses were conducted using the program CPPTRAJ of the AMBER 14 software suite.

Results

Comparison of XR and Kr2 structures

The three-dimensional structure of NaR, which is the primary object of investigation in this study, has not been determined. Therefore, we used its very similar carotenoid-deficient homologue, Kr2, for comparison with carotenoid-bound XR (Fig. 2). Both NaR and Kr2 are 280 amino acid residues in length, and their primary structures differ in only five residues found predominantly in loops on the protein surface at a distance from the presumed carotenoid-binding site (NaR/Kr2: Tyr88/Phe, Ser132/Thr, His159/Tyr, Lys190/Asn and Cys253/Ser). MD simulations of the modelled NaR structure confirmed its overall identity with the Kr2 structure (data not shown).

The XR sequence is seven residues shorter and displays only 29% identity with that of Kr2. Accordingly, their three-dimensional structures are similar but not identical. Their structures are superimposed in Fig. 2a based on two α-helices, αE and αF, which contain all protein ligands for the carotenoid. The XR-bound carotenoid fit well with the corresponding region of Kr2/NaR with only one exception:

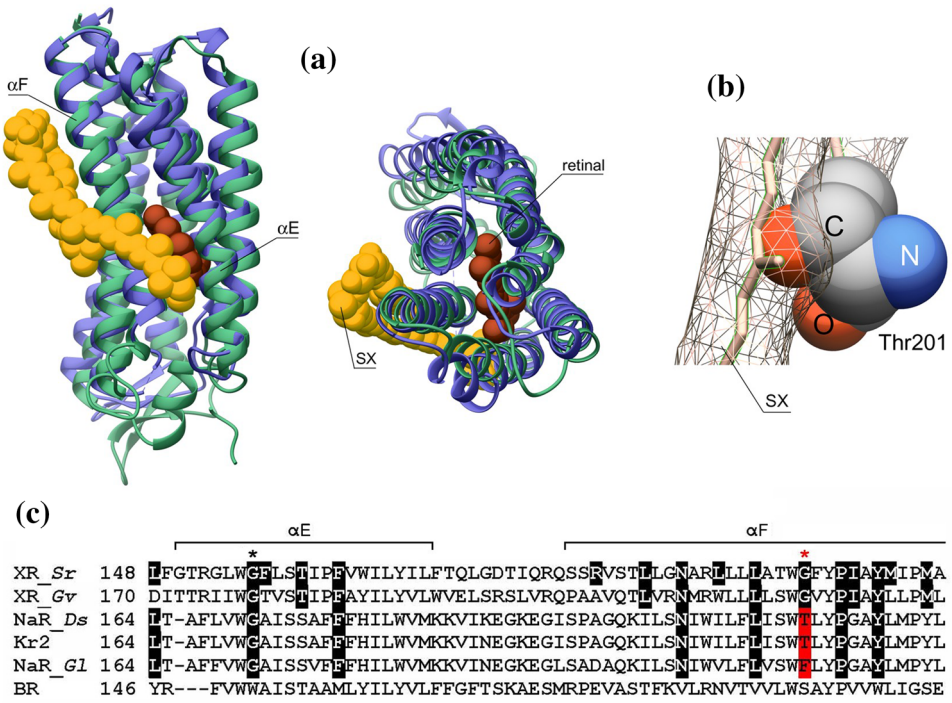

Fig. 2 Structural comparison of different rhodopsins. **a** Two views of the superimposition of the structures of Kr2 (PDB ID: 4XTL, coloured green) and carotenoid-bound XR (PDB ID: 3DDL, coloured violet) based on the α-helices αE and αF in both structures. SX and retinal in the XR structure are depicted as yellow orange and red spheres, respectively. **b** Clash between SX (shown as yellow orange sticks within its molecular surface indicated by mesh) and the Thr201 residue in the virtual Gly201Thr variant of XR. The most favourable Thr side chain rotamer is shown. **c** Partial sequence alignment of XRs from *S. ruber* (XR_*Sr*; GenBank accession code, ABC44767) and *G. violaceus* (XR_*Gv*; BAC88139); Na^+-translocating rhodopsins from *Dokdonia* sp. PRO95 (NaR_*Ds*; AEX55013), *K. eikastus* (Kr2; BAN14808) and *G. limnaea* (NaR_*Gl*; EHQ02967); and bacteriorhodopsin from *H. salinarum* (BR; AAA72504). Black boxes mark both the amino acid residues of XR_*Sr* involved in SX binding (Luecke et al. 2008) and the identical corresponding residues of other rhodopsins. The black asterisk marks the position of the Trp151 residue in BR, which was replaced by Gly in other rhodopsins; the red asterisk marks the position of the Gly-201/Thr216 residue in XR_*Sr*/NaR

the side chain of NaR Thr216 (corresponding to XR Gly201) overlapped with the SX polyene chain. This finding was verified by making a virtual Gly201Thr substitution in the XR three-dimensional structure. As illustrated in Fig. 2b, the side chain of the Thr residue markedly overlapped with the electron density of the bound SX molecule. Given its rigidity caused by conjugated double bonds, the Thr216 side chain is expected to interfere with carotenoid binding to NaR.

This inference is supported by comparison of the amino acid sequences of rhodopsins (Fig. 2c). Gly is found in the position of interest (marked with a red asterisk) in both carotenoid-bound rhodopsins (from *S. ruber* and *G. violaceus*) but is replaced by other residues in all rhodopsins for which carotenoid binding has not been demonstrated. Another substantial difference between both rhodopsin groups is that in the NaRs, Tyr replaces Met211 of XR. However, the analysis of the superimposed three-dimensional structures revealed no steric problems in carotenoid binding because of this replacement.

The importance of the Thr residue was verified by MD simulations of wild-type XR and its Gly201Thr variant complexed with SX. The proteins were placed into symmetrical bilayer membranes, and free energies were minimised to relieve any tension found in the crystal structure. The simulated structures displayed only small overall differences from the crystal structures (main chain root mean square deviation (RMSD) of 1.5–2 Å). However, a significant difference was observed in the carotenoid-binding region. In the crystal structure of wild-type XR, the distance between the retinal C3 atom and the oxygen atom of the antenna keto group is reasonably short (5.3 Å) for effective energy transfer from the carotenoid to the retinal. The distance was similar and stable in the simulated structure of wild-type XR (Fig. 3, black trace), whereas the distance increased abruptly to 10 Å in the variant XR shortly after starting the simulation (Fig. 3, red trace). This increase was required to prevent the clash between the carotenoid and the variant XR Thr201 that replaced Gly. The simulation was performed for only 200 ns and hence it could not be determined whether the carotenoid is eventually released from the complex. Nevertheless, these results strongly indicated that the Thr residue present in Kr2 and NaR in the position corresponding to XR

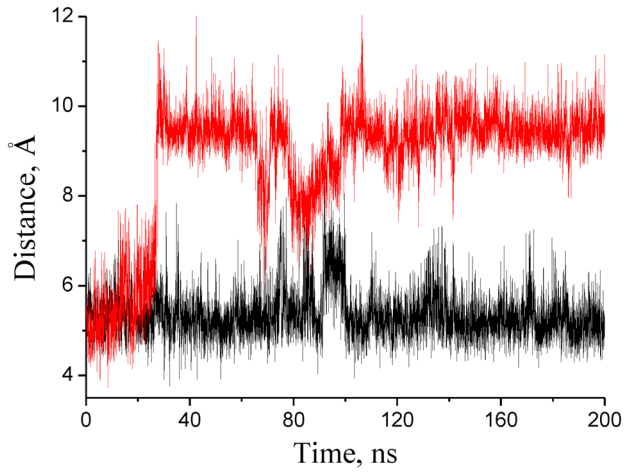

Fig. 3 Time course of the distance between retinal C3 and SX O21 atoms in *S. ruber* XR during the MD simulation. The black and red traces refer to wild-type XR and its Gly201Thr variant, respectively

Gly201 should interfere with carotenoid binding in a similar orientation to the retinal β-ionone ring.

Spectral probing of carotenoid binding to T216G-NaR

Based on the above prediction, a Thr216Gly variant of *Dokdonia* sp. PRO95 NaR was produced in *E. coli* and isolated using metal-chelating chromatography. The isolated protein contained no carotenoids, as indicated by the lack of carotenoid-specific absorption bands in the protein spectrum, which is consistent with the inability of *E. coli* cells to produce carotenoids.

XR-bound SX is an *S. ruber*-specific carotenoid (Lutnaes et al. 2002) and is unique because it contains a bulky acyl glycoside moiety (Fig. 1). We therefore decided to test more widespread ketocarotenoids such as ECN and CAN (Fig. 1), both of which lack this addition. To this effect, we coexpressed wild-type and variant NaR genes with the plasmid pACCAR25ΔcrtXZcrtO, which provides those *E. coli* cells the ability to synthesise ECN and CAN (Moldenhauer et al. 2017). Indeed, the absorption spectrum of T216G-NaR produced in this manner contained additional bands that had maxima at 430, 458 and 485 nm (Fig. 4a, red trace) compared with the spectrum of wild-type NaR produced in the same cells (blue trace). The form of the differential spectrum (Fig. 4a inset, black line) was characteristic of carotenoids (Britton et al. 2004), which indicated their presence in the variant NaR. Consistent with this conclusion, the NaR-bound carotenoids exhibited more resolved vibronic bands in this spectrum compared to the spectrum of unbound ECN/CAN (Fig. 4a inset, green line). Importantly, the spectra of wild-type NaR produced in the absence or presence of the pACCAR25ΔcrtXZcrtO plasmid were virtually identical,

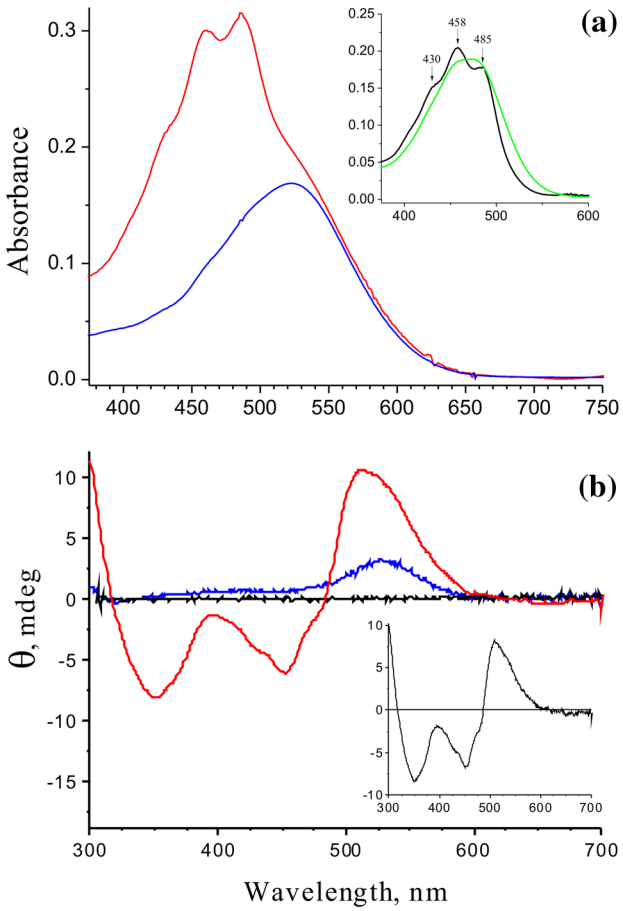

Fig. 4 Spectral detection of bound carotenoids in T216G-NaR. **a** Absorption spectroscopy. Wild-type (blue trace) and T216G variant (red trace) NaRs isolated from *E. coli* cells engineered to produce ECN and CAN. The spectra were recorded in 10 mM Tris-HEPES buffer (pH 8.0) that contained 100 mM KCl and 0.05% *n*-dodecyl β-D-maltoside (DDM), and a concentration of 3.5 μM NaR was used; cuvette path length was 10 mm. The inset shows the differential (red minus blue) spectrum (black trace) and the spectrum of isolated ECN/CAN in ethanol (green trace). **b** CD spectra of carotenoid-containing T216G-NaR (red trace), carotenoid-deficient T216G-NaR (blue trace) and ECN/CAN isolated from *E. coli* cells (black trace). The spectra of proteins were recorded in 10 mM Tris-HEPES buffer (pH 8.0) that contained 100 mM KCl and 0.05% DDM, and 6 μM protein was used; cuvette path length was 10 mm. The ECN/CAN spectrum was recorded in ethanol, and an ~3 μM concentration of carotenoids was used. The inset shows the differential (red minus blue) spectrum

which is in agreement with previous data (Bertsova et al. 2016).

Further evidence for the presence of specifically bound carotenoids in T216G-NaR isolated from carotenoid-producing cells was obtained using CD spectrometry. This protein exhibited an intense CD spectrum that had minima at 350 and 453 nm and maxima at < 300 and 512 nm (Fig. 4b), whereas the carotenoid-deficient T216G-NaR demonstrated only a weak positive signal at 525 nm,

which can be attributed to induced retinal chirality in its binding site. The carotenoid pool isolated from *E. coli*/pACCAR25ΔcrtXZcrtO/pRhod_T216G cells demonstrated no optical activity in the visible range, which is consistent with the absence of chiral atoms in the ECN and CAN structures.

Surprisingly, SX binding to T216G-NaR could not be demonstrated. Prolonged (2 h) incubation of purified T216G-NaR with a threefold molar excess of SX isolated from *S. ruber* followed by the removal of unbound SX by chromatography did not result in a significant increase in absorbance at 485 nm (data not shown), which is the absorbance maximum of SX (Imasheva et al. 2011). Furthermore, incubation of SX with T216G-NaR did not narrow the vibronic bands of the carotenoid in its optical absorption spectrum (data not shown), which was previously reported with respect to the carotenoid binding to *S. ruber* or *G. violaceus* XR (Balashov et al. 2006; Imasheva et al. 2009). SX binding to T216G-NaR is purportedly too weak to be detected in these in vitro tests.

Identification of T216G-NaR-bound carotenoids

Protein-bound carotenoids were extracted from T216G-NaR and identified using thin-layer chromatography simultaneously with the total pool of the carotenoids produced by *E. coli*/pACCAR25ΔcrtXZcrtO/pRhod_T216G cells. As shown in Fig. 5, ECN synthesis in the *E. coli*/pACCAR25ΔcrtXZcrtO/pRhod_T216G cells predominated over CAN synthesis, which is consistent with the specificity of the *Synechocystis* sp. PCC 6803 CrtO monoketolase, whose gene is present in the auxiliary plasmid used (Fernández-González et al. 1997; Moldenhauer et al. 2017). The distribution of T216G-NaR-bound carotenoids was opposite (Fig. 5), which suggests a higher affinity of the variant rhodopsin to CAN versus ECN. The carotenoid:retinal ratio could be estimated as ~0.5:1 from the spectra in Fig. 4 and from the known extinction coefficients for CAN and ECN; this ratio is half that for XR (Balashov et al. 2005). A likely explanation is that the bound carotenoids, especially ECN, were partly lost during rhodopsin isolation because of their lower affinity to T216G-NaR.

Carotenoid-to-retinal energy transfer in T216G-NaR

To work as an antenna, the bound carotenoid molecule must transmit accumulated energy to the retinal molecule. This property was tested by comparing the fluorescence excitation spectra of carotenoid-bound and carotenoid-deficient T216G-NaR. These measurements were conducted at pH 4.5 (i.e. under conditions favouring the protonation of the Schiff base counterion Asp116 and conversion of NaR into the 'blue' state (Gushchin et al. 2015) with a shift in the

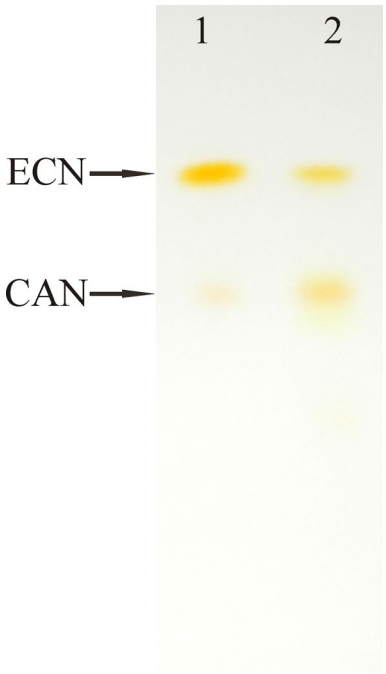

Fig. 5 Thin-layer chromatographic identification of the carotenoids produced by *E. coli*/pACCAR25ΔcrtXZcrtO/pRhod_T216G cells (lane 1) or bound to T216G-NaR isolated from those cells (lane 2)

retinal absorption maximum from 523 to 565 nm). The 'blue' form is characterised by increased fluorescence of retinal (Balashov et al. 2008) and better resolution of retinal and carotenoid spectra.

When excited at 565 nm, which is the wavelength of the maximal retinal absorption, carotenoid-bound and carotenoid-deficient T216G-NaR exhibited similar fluorescence emission spectra that had a wide maximum at approximately 660 nm (data not shown). In contrast, the fluorescence excitation spectra were markedly different (Fig. 6). The spectrum of the carotenoid-deficient T216G-NaR consisted of a single peak, which is attributed to retinal; however, the spectrum of the carotenoid-bound T216G-NaR exhibited additional bands in the short wavelength range with the maxima corresponding to carotenoid absorption. These findings are thus consistent with energy transfer from carotenoids to retinal, highlighting the antenna role of the carotenoids in T216G-NaR. The efficiency of energy transfer from carotenoids to retinal in T216G-NaR could be estimated according to Balashov et al. (2008) from the absorption and fluorescence excitation spectra (Figs. 4a, 6, respectively) as ~30%.

Photocycle parameters in T216G-NaR

The photocycle of the wild-type and variant NaRs was measured at low and high Na^+ concentrations using flash photolysis by monitoring absorbance changes at 605 nm. Using this

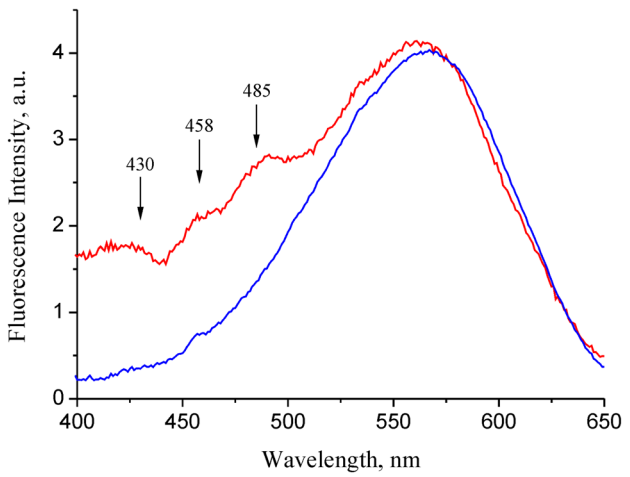

Fig. 6 Fluorescence excitation spectra of carotenoid-containing T216G-NaR (red trace) and carotenoid-deficient T216G-NaR (blue trace). Emissions were detected at 670 nm in 100 mM sodium acetate buffer (pH 4.5) that contained 0.05% DDM, and concentrations of 1 µM protein were used. The arrows indicate the positions of the maxima observed in the absorption spectrum (Fig. 4a, inset)

wavelength allows the detection of all transmissions between the reaction intermediates in NaR (Mamedov et al. 2016). The wild-type NaR photocycle includes the following major steps: $NaR \xrightarrow{h\nu} K \rightarrow (L \leftrightarrow M) \rightarrow O \rightarrow NaR$ (Inoue et al. 2013; Bogachev et al. 2016). The characteristic times for the decay of the intermediate *K*, the formation of the intermediate *O* and the decay of *O* for wild-type NaR in the presence of 100 mM Na^+ at pH 8.0 were 0.025, 1.3 and 10 ms, respectively (Fig. 7a). The corresponding times for the carotenoid-bound T216G-NaR were very similar—0.025, 1.4 and 11 ms (Fig. 7a)—as were those for the carotenoid-deficient T216G-NaR (data not shown). Intermediate *O* formation was markedly decelerated at low Na^+ concentration, resulting in its lower accumulation during the photocycle (Fig. 7b). All three forms of NaR were equally sensitive to Na^+ concentration. These results indicated that the amino acid replacement and bound carotenoids did not influence NaR functionality.

Discussion

We have previously demonstrated that *Dokdonia* sp. PRO95 NaR binds neither endogenous carotenoids nor the exogenous ketocarotenoid SX (Bertsova et al. 2016). These results were confirmed in the present study, indicating that unlike its close homologues (H^+-pumping XRs), NaR contains no carotenoid antenna. Structural comparisons in combination with MD simulations have revealed a Thr residue (Thr216) that likely interferes with carotenoid polyene chain binding in NaR. In XR, Gly occupies the corresponding position. The α-helical location of these residues in the two proteins strongly suggests that the size of their side chain matters more rather than the variability of the dihedral angles.

This finding prompted a simple site-directed mutagenesis experiment in which Gly replaced Thr216 in NaR. The replacement did confer to NaR the ability to bind in vivo the ketocarotenoids CAN and ECN in the *E. coli* strain engineered to produce these carotenoids. The binding was specific, as indicated by the fine structure of the absorption spectrum (Fig. 4a) and the appearance of a CD spectrum (Fig. 4b). The differential CD spectrum of carotenoid-bound T216G-NaR exhibited nearly equal amplitudes of

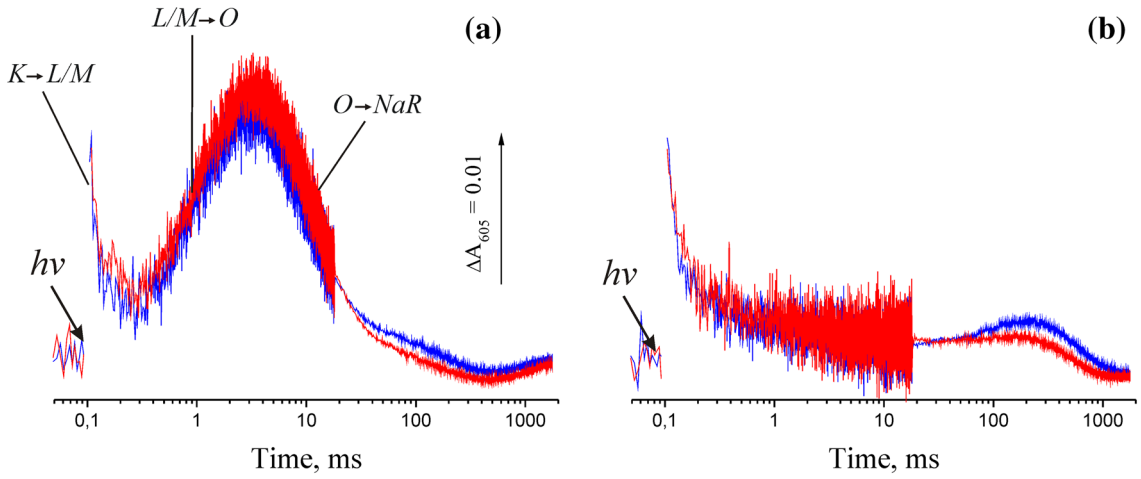

Fig. 7 Kinetics of absorbance changes at 605 nm during the photocycle of wild-type NaR (blue traces) and carotenoid-containing T216G-NaR (red traces). The assay medium contained 18 µM rhodopsin protein, 100 mM NaCl **a** or 100 mM KCl **b**; 0.05% DDM; and 20 mM Tris-HEPES (pH 8.0). The arrow indicates the laser flash. The transitions involved are marked for the NaCl-containing medium only. The Na^+ concentration of the KCl-containing medium was 35 µM

the positive and negative lobes in the long-wavelength region, suggesting its origination from excitonic coupling between the carotenoids and retinal (Balashov et al. 2006; Fujimoto and Balashov 2017) or between the carotenoids bound to different subunits (Smolensky Koganov et al. 2015). Noteworthy in this regard, NaR is capable of forming pentameric structures (Gushchin et al. 2015). Alternatively, the CD spectrum may result from binding-induced carotenoid chirality (Balashov et al. 2006). In any case, the mere existence of an intense CD spectrum is indicative of specificity in the carotenoid binding to T216G-NaR. Interestingly, the CD spectrum of carotenoid-bound T216G-NaR mirrored that of XR (Balashov et al. 2006) relative to the wavelength axis. This finding suggests that different dihedral angles occur between the electric transition moments of interacting chromophores in T216G-NaR and XR, as changes in their values can result in CD spectrum inversion if the interaction is excitonic in nature (Tinoco 1963).

Bound carotenoids can transmit light energy to retinal (i.e. bound carotenoids can function as a light-harvesting antenna in T216G-NaR, as indicated by the fluorescence excitation spectrum) (Fig. 6). The contribution of the carotenoids to retinal fluorescence excitation in T216G-NaR was somewhat less than that of *S. ruber* and *G. violaceus* XRs (Balashov et al. 2008, 2010), which is consistent with the lower efficiency of energy transfer from carotenoids to retinal in T216G-NaR (~ 30%) than in XR (~ 45%) (Balashov et al. 2008). Nevertheless, the bound carotenoids significantly increased the efficiency of light harvesting in NaR.

The ability of XRs to bind carotenoids was previously associated with the replacement of the bulky Trp151 found in carotenoid-deficient bacteriorhodopsin precursors by a Gly residue (Gly156 in *S. ruber* XR in Fig. 2c) (Luecke et al. 2008). This replacement results in the creation of a hydrophobic cavity accommodating the SX keto ring near the retinal β-ionone ring. A reverse Gly-to-Trp substitution abolished SX binding in XR (Balashov et al. 2010). Our data revealed that a glycine residue, Gly201, which is in close proximity to the carotenoid polyene chain in XR (Luecke et al. 2008; Imasheva et al. 2009), is essential for carotenoid binding in XR and antenna engineering into NaR. Interestingly, both key residues for carotenoid binding are Gly. It therefore seems that the evolutionary path to antenna-containing rhodopsins simply involved the replacements of two bulky residues by small Gly residues.

Knowing the key role of Gly201 in carotenoid binding allows a more reliable prediction of the in vivo antenna function in rhodopsins. Based on the presence of Thr or Phe in the corresponding position in Kr2 and *Gillisia limnaea* NaR (Fig. 2c), these rhodopsins are expected to have no carotenoid antenna. Similarly, Subgroup II XRs have in this position residues other than Gly, supporting a previous hypothesis regarding their lack of antenna (Vollmers et al. 2013).

The fact that only one replacement suffices to enable the ability to bind the carotenoid antenna may indicate that the NaR rhodopsin ancestor contained such an antenna but that this antenna was lost during the evolutionary pathway to NaR. This generates a natural question: why was such a functionally important and evolutionarily advantageous trait lost during evolution? A trivial explanation is that the rhodopsins that initially contained antenna were horizontally transferred to flavobacteria that lacked a ketocarotenoid-synthesising pathway. Indeed, none of the flavobacterial carotenoids contain a cyclohexanone ring keto group (Bertsova et al. 2016), which is essential for binding to rhodopsins (Balashov et al. 2010; Imasheva et al. 2011). Thereafter, a structure-stabilising Gly-to-Thr point mutation could have occurred. The identity of the residue occupying the corresponding position is important for carotenoid binding in XRs but not for photocycle performance (Fig. 7). Similarly, a Ser-to-Ala replacement in the same position of *H. salinarum* bacteriorhodopsin did not affect the functional properties of the bacteriorhodopsin (Ahl et al. 1989; Marti et al. 1991). Additional studies should help clarify the adaptation-justified reason for the loss of carotenoid antennae in the NaRs and many XRs. Such studies will also reveal whether the carotenoid-binding form was ancestral to the whole family of microbial rhodopsins or the ability to bind carotenoids has developed only in one particular branch of rhodopsins.

Acknowledgements This work was supported by the Russian Science Foundation Research Project 14-14-00128. We are indebted to Prof. T. Friedrich for providing us the pACCAR25ΔcrtXZcrtO plasmid and for helpful discussions.

Compliance with ethical standards

Conflict of interest The authors declare that they have no conflict of interest.

References

Ahl PL, Stern LJ, Mogi T, Khorana HG, Rothschild KJ (1989) Substitution of amino acids in helix F of bacteriorhodopsin: effects on the photochemical cycle. Biochemistry 28:10028–10034

Balashov SP, Imasheva ES, Boichenko VA, Antón J, Wang JM, Lanyi JK (2005) Xanthorhodopsin: a proton pump with a light-harvesting carotenoid antenna. Science 309:2061–2064

Balashov SP, Imasheva ES, Lanyi JK (2006) Induced chirality of the light-harvesting carotenoid salinixanthin and its interaction with the retinal of xanthorhodopsin. Biochemistry 45:10998–11004

Balashov SP, Imasheva ES, Wang JM, Lanyi JK (2008) Excitation energy-transfer and the relative orientation of retinal and carotenoid in xanthorhodopsin. Biophys J 95:2402–2414

Balashov SP, Imasheva ES, Choi AR, Jung KH, Liaaen-Jensen S, Lanyi JK (2010) Reconstitution of Gloeobacter rhodopsin with echinenone: role of the 4-keto group. Biochemistry 49:9792–9799

Bertsova YV, Bogachev AV, Skulachev VP (2015) Proteorhodopsin from *Dokdonia* sp. PRO95 is a light-driven Na^+-pump. Biochemistry (Moscow) 80:449–454

Bertsova YV, Arutyunyan AM, Bogachev AV (2016) Na^+-translocating rhodopsin from *Dokdonia* sp. PRO95 does not contain carotenoid antenna. Biochemistry (Moscow) 81:414–419

Bogachev AV, Bertsova YV, Verkhovskaya ML, Mamedov MD, Skulachev VP (2016) Real-time kinetics of electrogenic Na^+ transport by rhodopsin from the marine flavobacterium *Dokdonia sp*. PRO95. Sci Rep 6:21397

Boichenko VA, Wang JM, Antón J, Lanyi JK, Balashov SP (2006) Functions of carotenoids in xanthorhodopsin and archaerhodopsin from action spectra of photoinhibition of cell respiration. Biochim Biophys Acta 1757:1649–1656

Britton G, Liaaen-Jensen S, Pfander H (2004) Carotenoids handbook, Birkhauser Verlag AG, Basel

Case DA, Babin V, Berryman JT, Betz RM, Cai Q, Cerutti DS, Cheatham TE III, Darden TA, Duke RE, Gohlke H, Goetz AW, Gusarov S, Homeyer N, Janowski P, Kaus J, Kolossváry I, Kovalenko A, Lee TS, LeGrand S, Luchko T, Luo R, Madej B, Merz KM, Paesani F, Roe DR, Roitberg A, Sagui C, Salomon-Ferrer R, Seabra G, Simmerling CL, Smith W, Swails J, Walker RC, Wang J, Wolf RM, Wu X, Kollman PA (2014) AMBER 14. University of California, San Francisco

Croce R, van Amerongen H (2014) Natural strategies for photosynthetic light harvesting. Nat Chem Biol 10:492–501

Fernández-González B, Sandmann G, Vioque A (1997) A new type of asymmetrically acting β-carotene ketolase is required for the synthesis of echinenone in the cyanobacterium *Synechocystis* sp PCC 6803. J Biol Chem 272:9728–9733

Fujimoto KJ, Balashov SP (2017) Vibronic coupling effect on circular dichroism spectrum: carotenoid–retinal interaction in xanthorhodopsin. J Chem Phys 146:095101–095106

Gushchin I, Shevchenko V, Polovinkin V, Kovalev K, Alekseev A, Round E, Borshchevskiy V, Balandin T, Popov A, Gensch T, Fahlke C, Bamann C, Willbold D, Büldt G, Bamberg E, Gordeliy V (2015) Crystal structure of a light-driven sodium pump. Nat Struct Mol Biol 22:390–395

Hsieh LK, Lee TC, Chichester CO, Simpson KL (1974) Biosynthesis of carotenoids in *Brevibacterium* sp. KY-4313. J Bacteriol 118:385–393

Imasheva ES, Balashov SP, Wang JM, Smolensky E, Sheves M, Lanyi JK (2008) Chromophore interaction in xanthorhodopsin—retinal dependence of salinixanthin binding. Photochem Photobiol 84:977–984

Imasheva ES, Balashov SP, Choi AR, Jung KH, Lanyi JK (2009) Reconstitution of *Gloeobacter violaceus* rhodopsin with a light-harvesting carotenoid antenna. Biochemistry 48:10948–10955

Imasheva ES, Balashov SP, Wang JM, Lanyi JK (2011) Removal and reconstitution of the carotenoid antenna of xanthorhodopsin. J Membr Biol 239:95–104

Inoue K, Ono H, Abe-Yoshizumi R, Yoshizawa S, Ito H, Kogure K, Kandori H (2013) A light-driven sodium ion pump in marine bacteria. Nat Commun 4:1678

Jo S, Kim T, Iyer VG, Im W (2008) CRHARMM-GUI: a web-based graphical user interface for CHARMM. J Comput Chem 29:1859–1865

Kato HE, Inoue K, Abe-Yoshizumi R, Kato Y, Ono H, Konno M, Hososhima S, Ishizuka T, Hoque MR, Kunitomo H, Ito J, Yoshizawa S, Yamashita K, Takemoto M, Nishizawa T, Taniguchi R, Kogure K, Maturana AD, Iino Y, Yawo H, Ishitani R, Kandori H, Nureki O (2015) Structural basis for Na^+ transport mechanism by a light-driven Na^+ pump. Nature 521:48–53

Luecke H, Schobert B, Stagno J, Imasheva ES, Wang JM, Balashov SP, Lanyi JK (2008) Crystallographic structure of xanthorhodopsin the light-driven proton pump with a dual chromophore. Proc Natl Acad Sci USA 105:16561–16565

Lutnaes BF, Oren A, Liaaen-Jensen S (2002) New C_{40}-carotenoid acyl glycoside as principal carotenoid in *Salinibacter ruber*, an extremely halophilic eubacterium. J Nat Prod 65:1340–1343

Mamedov MD, Mamedov AM, Bertsova YV, Bogachev AV (2016) A single mutation converts bacterial Na^+-transporting rhodopsin into an H^+ transporter. FEBS Lett 590:2827–2835

Marti T, Otto H, Mogi T, Rösselet SJ, Heyn MP, Khorana HG (1991) Bacteriorhodopsin mutants containing single substitutions of serine or threonine residues are all active in proton translocation. J Biol Chem 266:6919–6927

Moldenhauer M, Sluchanko NN, Buhrke D, Zlenko DV, Tavraz NN, Schmitt FJ, Hildebrandt P, Maksimov EG, Friedrich T (2017) Assembly of photoactive orange carotenoid protein from its domains unravels a carotenoid shuttle mechanism. Photosynth Res 133:327–341

Pettersen EF, Goddard TD, Huang CC, Couch GS, Greenblatt DM, Meng EC, Ferrin TE (2004) UCSF Chimera—a visualization system for exploratory research and analysis. J Comput Chem 25:1605–1612

Smolensky Koganov E, Brumfeld V, Friedman N, Sheves M (2015) Origin of circular dichroism of xanthorhodopsin. A study with artificial pigments. J Phys Chem B 119:456–464

Tinoco I (1963) The exciton contribution to the optical rotation of polymers. Radiat Res 20:133–139

Vollmers J, Voget S, Dietrich S, Gollnow K, Smits M, Meyer K, Brinkhoff T, Simon M, Daniel R (2013) Poles apart: arctic and Antarctic *Octadecabacter* strains share high genome plasticity and a new type of xanthorhodopsin. PLoS ONE 8:e63422